Rethinking the Faster R-CNN Architecture for Temporal Action Localization

Yu-Wei Chao[1*], Sudheendra Vijayanarasimhan[2], Bryan Seybold[2], David A. Ross[2], Jia Deng[1], Rahul Sukthankar[2]

[1]University of Michigan, Ann Arbor
{ywchao,jiadeng}@umich.edu

[2]Google Research
{svnaras,seybold,dross,sukthankar}@google.com

Abstract

We propose TAL-Net, an improved approach to temporal action localization in video that is inspired by the Faster R-CNN object detection framework. TAL-Net addresses three key shortcomings of existing approaches: (1) we improve receptive field alignment using a multi-scale architecture that can accommodate extreme variation in action durations; (2) we better exploit the temporal context of actions for both proposal generation and action classification by appropriately extending receptive fields; and (3) we explicitly consider multi-stream feature fusion and demonstrate that fusing motion late is important. We achieve state-of-the-art performance for both action proposal and localization on THUMOS'14 detection benchmark and competitive performance on ActivityNet challenge.

1. Introduction

Visual understanding of human actions is a core capability in building assistive AI systems. The problem is conventionally studied in the setup of action classification [46, 37, 30], where the goal is to perform forced-choice classification of a temporally trimmed video clip into one of several action classes. Despite fruitful progress, this classification setup is unrealistic, because real-world videos are usually untrimmed and the actions of interest are typically embedded in a background of irrelevant activities. Recent research attention has gradually shifted to temporal action localization in untrimmed video [24, 32, 47], where the task is to not only identify the action class, but also detect the start and end time of each action instance. Improvements in temporal action localization can drive progress on a large number of important topics ranging from immediate applications, such as extracting highlights in sports video, to higher-level tasks, such as automatic video captioning.

Temporal action localization, like object detection, falls under the umbrella of visual detection problems. While object detection aims to produce spatial bounding boxes in a 2D image, temporal action localization aims to produce temporal segments in a 1D sequence of frames. As a result, many approaches to action localization have drawn inspiration from advances in object detection. A successful example is the use of region-based detectors [18, 17, 33]. These methods first generate a collection of class-agnostic region proposals from the full image, and go through each proposal to classify its object class. To detect actions, one can follow this paradigm by first generating segment proposals from the full video, followed by classifying each proposal.

Among region-based detectors, Faster R-CNN [33] has been widely adopted in object detection due to its competitive detection accuracy on public benchmarks [28, 13]. The core idea is to leverage the immense capacity of deep neural networks (DNNs) to power the two processes of proposal generation and object classification. Given its success in object detection in images, there is considerable interest in employing Faster R-CNN for temporal action localization in video. However, such a domain shift introduces several challenges. We review the issues of Faster R-CNN in the action localization domain, and redesign the architecture to specifically address them. We focus on the following:

1. **How to handle large variations in action durations?** The temporal extent of actions varies dramatically compared to the size of objects in an image—from a fraction of a second to minutes. However, Faster R-CNN evaluates different scales of candidate proposals (i.e., anchors) based on a shared feature representation, which may not capture relevant information due to a misalignment between the temporal scope of the feature (i.e. receptive field) and the span of the anchor. We propose to enforce such alignment using a multi-tower network and dilated temporal convolutions.
2. **How to utilize temporal context?** The moments preceding and following an action instance contain critical information for localization and classification (arguably more so than the spatial context of an object). A naive application of Faster R-CNN would fail to exploit this temporal context. We propose to explicitly encode temporal context by extending the receptive fields in proposal generation and action classification.

*Work done in part during an internship at Google Research.

3. **How best to fuse multi-stream features?** State-of-the-art action classification results are mostly achieved by fusing RGB and optical flow based features. However, there has been limited work in exploring such feature fusion for Faster R-CNN. We propose a late fusion scheme and empirically demonstrate its edge over the common early fusion scheme.

Our contributions are twofold: (1) we introduce the Temporal Action Localization Network (TAL-Net), which is a new approach for action localization in video based on Faster R-CNN; (2) we achieve state-of-the-art performance on both action proposal and localization on the THUMOS'14 detection benchmark [22], along with competitive performance on the ActivityNet dataset [5].

2. Related Work

Action Recognition Action recognition is conventionally formulated as a classification problem. The input is a video that has been temporally trimmed to contain a specific action of interest, and the goal is to classify the action. Tremendous progress has recently been made due to the introduction of large datasets and the developments on deep neural networks [37, 30, 43, 49, 7, 14]. However, the assumption of trimmed input limits the application of these approaches in real scenarios, where the videos are usually untrimmed and may contain irrelevant backgrounds.

Temporal Action Localization Temporal action localization assumes the input to be a long, untrimmed video, and aims to identify the start and end times as well as the action label for each action instance in the video. The problem has recently received significant research attention due to its potential application in video data analysis. Below we review the relevant work on this problem.

Early approaches address the task by applying temporal sliding windows followed by SVM classifiers to classify the action within each window [24, 32, 47, 31, 54]. They typically extract improved dense trajectory [46] or pre-trained DNN features, and globally pool these features within each window to obtain the input for the SVM classifiers. Instead of global pooling, Yuan et al. [54] proposed a multi-scale pooling scheme to capture features at multiple resolutions. However, these approaches might be computationally inefficient, because one needs to apply each action classifier exhaustively on windows of different sizes at different temporal locations throughout the entire video.

Another line of work generates frame-wise or snippet-wise action labels, and uses these labels to define the temporal boundaries of actions [29, 38, 10, 26, 55, 20]. One major challenge here is to enable temporal contextual reasoning in predicting the individual labels. Lea et al. [26] proposed novel temporal convolutional architectures to capture long-range temporal dependencies, while others [29, 38, 10] use recurrent neural networks. A few other methods add a separate contextual reasoning stage on top of the frame-wise or snippet-wise prediction scores to explicitly model action durations or temporal transitions [34, 55, 20].

Inspired by the recent success of region-based detectors in object detection [18, 17], many recent approaches adopt a two-stage, proposal-plus-classification framework [6, 36, 12, 3, 4, 35, 56], i.e. first generating a sparse set of class-agnostic segment proposals from the input video, followed by classifying the action categories for each proposal. A large number of these works focus on improving the segment proposals [6, 12, 4, 3], while others focus on building more accurate action classifiers [35, 56]. However, most of these methods do not afford end-to-end training on either the proposal or classification stage. Besides, the proposals are typically selected from sliding windows of predefined scales [36], where the boundaries are fixed and may result in imprecise localization if the windows are not dense.

As the latest incarnation of the region-based object detectors, the Faster R-CNN architecture [33] is composed of end-to-end trainable proposal and classification networks, and applies region boundary regression in both stages. A few very recent works have started to apply such architecture to temporal action localization [15, 9, 16, 51], and demonstrated competitive detection accuracy. In particular, the R-C3D network [51] is a classic example that closely follows the original Faster R-CNN in many design details. While being a powerful detection paradigm, we argue that naively applying the Faster R-CNN architecture to temporal action localization might suffer from a few issues. We propose to address these issues in this paper. We will also clarify our contributions over other Faster R-CNN based methods [15, 9, 16, 51] later when we introduce TAL-Net.

In addition to the works reviewed above, there exist other classes of approaches, such as those based on single-shot detectors [2, 27] or reinforcement learning [52]. Others have also studied temporal action localization in a weakly supervised setting [41, 48], where only video-level action labels are available for training. Also note that besides temporal action localization, there also exists a large body of work on spatio-temporal action localization [19, 23, 40], which is beyond the scope of this paper.

3. Faster R-CNN

We briefly review the Faster R-CNN detection framework in this section. Faster R-CNN is first proposed to address object detection [33], where given an input image, the goal is to output a set of detection bounding boxes, each tagged with an object class label. The full pipeline consists of two stages: *proposal generation* and *classification*. First, the input image is processed by a 2D ConvNet to generate a 2D feature map. Another 2D ConvNet (referred to as the Region Proposal Network) is then used to generate

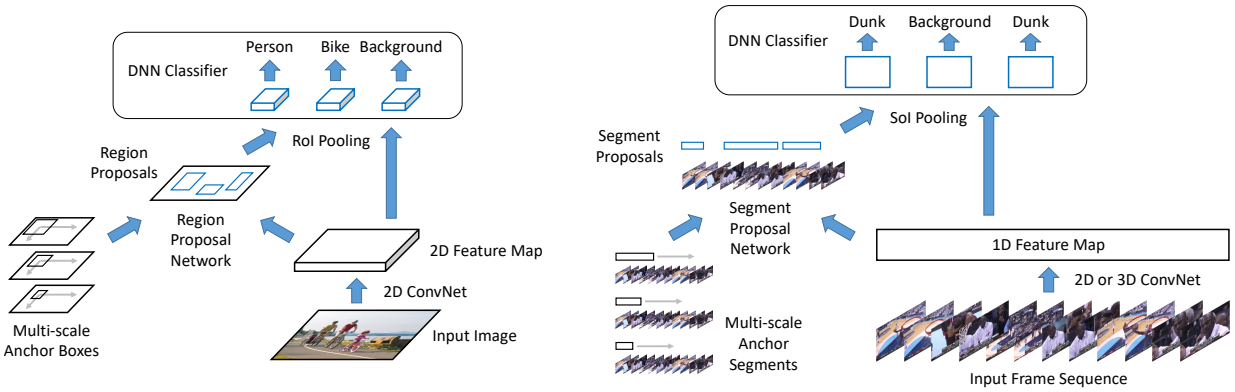

Figure 1: Contrasting the Faster R-CNN architecture for object detection in images [33] (left) and temporal action localization in video [15, 9, 16, 51] (right). Temporal action localization can be viewed as the 1D counterpart of the object detection problem.

a sparse set of class-agnostic region proposals, by classifying a group of scale varying anchor boxes centered at each pixel location of the feature map. The boundaries of the proposals are also adjusted with respect to the anchor boxes through regression. Second, for each region proposal, features within the region are first pooled into a fixed size feature map (i.e. RoI pooling [17]). Using the pooled feature, a DNN classifier then computes the object class probabilities and simultaneously regresses the detection boundaries for each object class. Fig. 1 (left) illustrates the full pipeline. The framework is conventionally trained by alternating between the training of the first and second stage [33].

Faster R-CNN naturally extends to temporal action localization [15, 9, 51]. Recall that object detection aims to detect 2D spatial regions, whereas in temporal action localization, the goal is to detect 1D temporal *segments*, each represented by a *start* and an *end* time. Temporal action localization can thus be viewed as the 1D counterpart of object detection. A typical Faster R-CNN pipeline for temporal action localization is illustrated in Fig. 1 (right). Similar to object detection, it consists of two stages. First, given a sequence of frames, we extract a 1D feature map, typically via a 2D or 3D ConvNet. The feature map is then passed to a 1D ConvNet [1] (referred to as the Segment Proposal Network) to classify a group of scale varying anchor segments at each temporal location, and also regress their boundaries. This returns a sparse set of class-agnostic segment proposals. Second, for each segment proposal, we compute the action class probabilities and further regress the segment boundaries, by first applying a 1D RoI pooling (termed "SoI pooling") layer followed by a DNN classifier.

4. TAL-Net

TAL-Net follows the Faster R-CNN detection paradigm for temporal action localization (Fig. 1 right) but features three novel architectural changes (Sec. 4.1 to 4.3).

4.1. Receptive Field Alignment

Recall that in proposal generation, we generate a sparse set of class-agnostic proposals by classifying a group of scale varying anchors at each location in the feature map. In object detection [33], this is achieved by applying a small ConvNet on top of the feature map, followed by a 1×1 convolutional layers with K filters, where K is the number of scales. Each filter will classify the anchor of a particular scale. This reveals an important *limitation*: the anchor classifiers at each location share the same receptive field. Such design may be reasonable for object detection, but may not generalize well to temporal action localization, because the temporal length of actions can vary more drastically compared to the spatial size of objects, e.g. in THUMOS'14 [22], the action lengths range from less than a second to more than a minute. To ensure a high recall, the applied anchor segments thus need to have a wide range of scales (Fig. 2 left). However, if the receptive field is set too small (i.e. temporally short), the extracted feature may not contain sufficient information when classifying large (i.e. temporally long) anchors, while if it is set too large, the extracted feature may be dominated by irrelevant information when classifying small anchors.

To address this issue, we propose to align each anchor's receptive field with its temporal span. This is achieved by two key enablers: a *multi-tower* network and *dilated temporal convolutions*. Given a 1D feature map, our Segment Proposal Network is composed of a collection of K temporal ConvNets, each responsible for classifying the anchor segments of a particular scale (Fig. 2 right). Most importantly, each temporal ConvNet is carefully designed such that its receptive field size coincides with the associated anchor scale. At the end of each ConvNet, we apply two parallel convolutional layers with kernel size 1 for anchor classification and boundary regression, respectively.

[1] "1D convolution" & "temporal convolution" are used interchangeably.

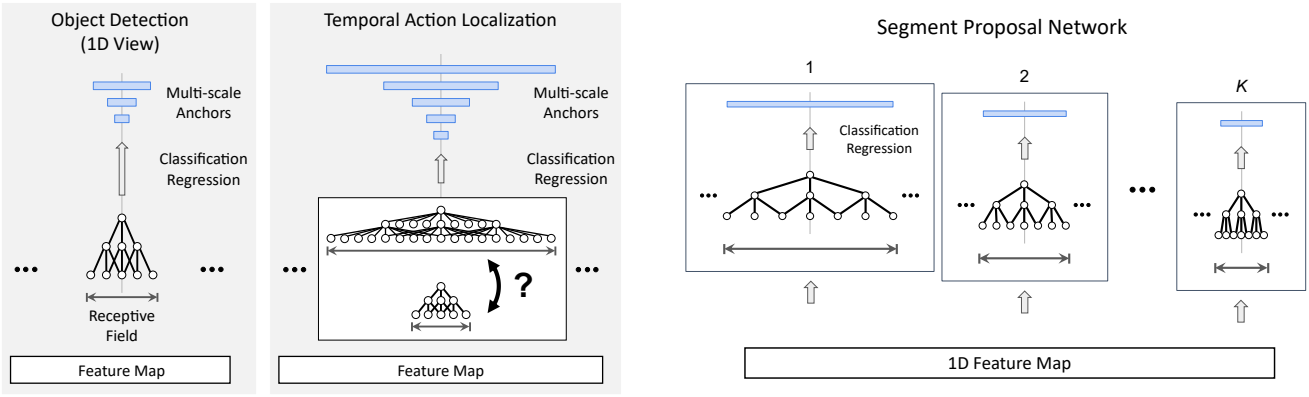

Figure 2: Left: The limitation of sharing the receptive field across different anchor scales in temporal action localization. Right: The multi-tower architecture of our Segment Proposal Network. Each anchor scale has an associated network with aligned receptive field.

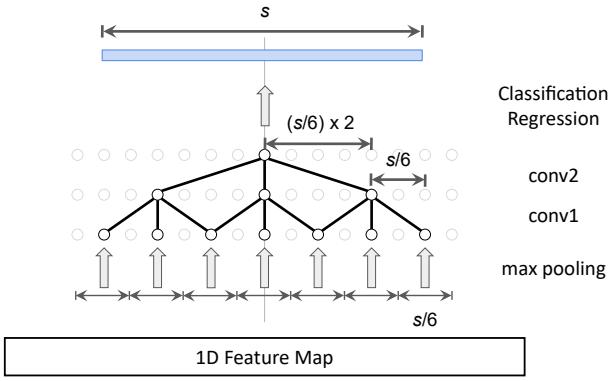

Figure 3: Controlling the receptive field size s with dilated temporal convolutions.

The next question is: how do we design temporal ConvNets with a controllable receptive field size s? Suppose we use temporal convolutional filters with kernel size 3 as a building block. One way to increase s is simply stacking the convolutional layers: $s = 2L + 1$ if we stack L layers. However, given a target receptive field size s, the required number of layers L will then grow linearly with s, which can easily increase the number of parameters and make the network prone to overfitting. One solution is to apply pooling layers: if we add a pooling layer with kernel size 2 after each convolutional layer, the receptive field size is then given by $s = 2^{(L+1)} - 1$. While now L grows logarithmically with s, the added pooling layers will exponentially reduce the resolution of the output feature map, which may sacrifice localization precision in detection tasks.

To avoid overgrowing the model while maintaining the resolution, we propose to use dilated temporal convolutions. Dilated convolutions [8, 53] act like regular convolutions, except that one subsamples pixels in the input feature map instead of taking adjacent ones when multiplied with a convolution kernel. This technique has been successfully applied to 2D ConvNets [8, 53] and 1D ConvNets [26] to expand the receptive field without loss of resolution. In our Segment Proposal Network, each temporal ConvNet consists of only two dilated convolutional layers (Fig. 3). To attain a target receptive field size s, we can explicitly compute the required dilation rate (i.e. subsampling rate) r_l for layer l by $r_1 = s/6$ and $r_2 = (s/6) \times 2$. We also smooth the input before subsampling by adding a max pooling layer with kernel size $s/6$ before the first convolutional layer.

Contributions beyond [9, 15, 16, 51] Xu et al. [51] followed the original Faster R-CNN and thus their anchors at each pixel location still shared the receptive field. Both Gao et al. [15, 16] and Dai et al. [9] aligned each anchor's receptive field with its span. However, Gao et al. [15, 16] average pooled the features within the span of each anchor, whereas we use temporal convolutions to extract structure-sensitive features. Our approach is similar in spirit to Dai et al. [9], which sampled a fixed number of features within the span of each anchor; we approach this using dilated convolutions.

4.2. Context Feature Extraction

Temporal context information (i.e. what happens immediately before and after an action instance) is a critical signal for temporal action localization for two reasons. First, it enables more accurate localization of the action boundaries. For example, seeing a person standing still on the far end of a diving board is a strong signal that he will soon start a "diving" action. Second, it provides strong semantic cues for identifying the action class within the boundaries. For example, seeing a javelin flying in the air indicates that a person just finished a "javelin throw", not "pole vault". As a result, it is critical to encode the temporal context features in the action localization pipeline. Below we detail our approach to explicitly exploit context features in both the proposal generation and action classification stage.

In proposal generation, we showed the receptive field for classifying an anchor can be matched with the anchor's span (Sec. 4.1). However, this only extracts the features within

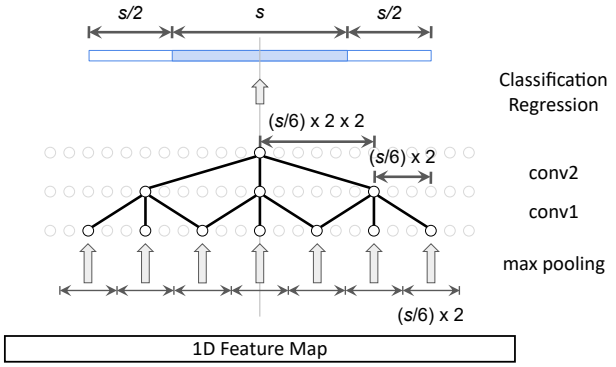

Figure 4: Incorporating context features in proposal generation.

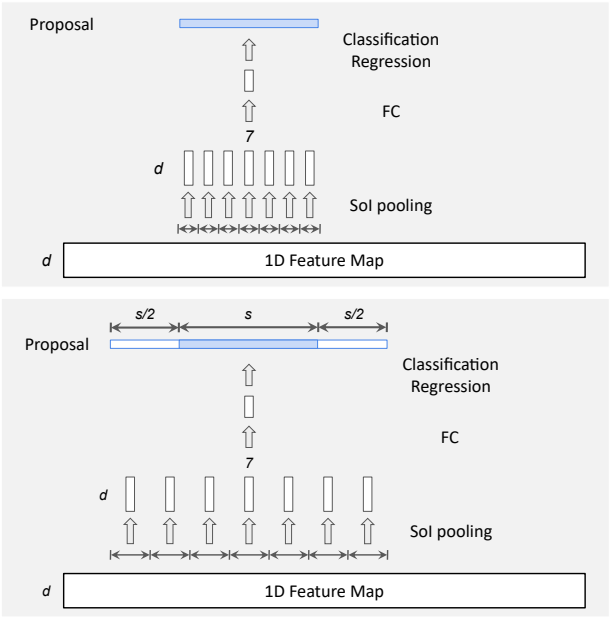

Figure 5: Classifying a proposal without (top) [17, 33] and with (bottom) incorporating context features

the anchor, and overlooks the contexts before and after it. To ensure the context features are used for anchor classification and boundary regression, the receptive field must cover the context regions. Suppose the anchor is of scale s, we enforce the receptive field to also cover the two segments of length $s/2$ immediately before and after the anchor. This can be achieved by doubling the dilation rate of the convolutional layers, i.e. $r_1 = (s/6) \times 2$ and $r_2 = (s/6) \times 2 \times 2$, as illustrated in Fig. 4. Consequently, we also double the kernel size of the initial max pooling layer to $(s/6) \times 2$.

In action classification, we perform SoI pooling (i.e. 1D RoI pooling) to extract a fixed size feature map for each obtained proposal. We illustrate the mechanism of SoI pooling with output size 7 in Fig. 5 (top). Note that as in the original design of RoI pooling [17, 33], pooling is applied to the region strictly within the proposal, which includes no temporal contexts. We propose to extend the input extent of SoI pooling. As shown in Fig. 5 (bottom), for a proposal of size s, the extent of our SoI pooling covers not only the proposal segment, but also the two segments of size $s/2$ immediately before and after the proposal, similar to the classification of anchors. After SoI pooling, we add one fully-connected layer, followed by a final fully-connected layer, which classifies the action and regresses the boundaries.

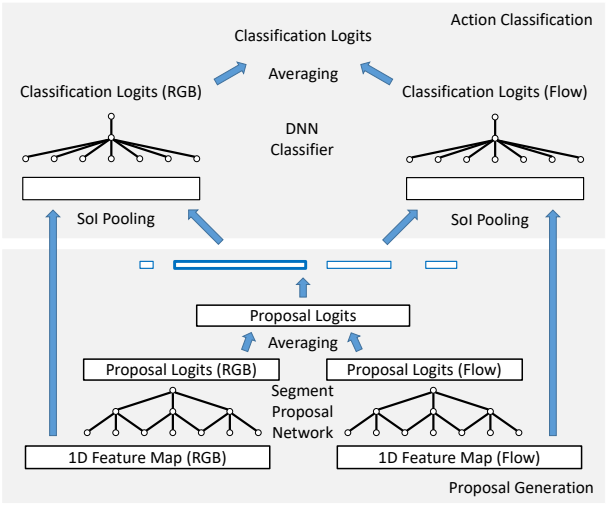

Figure 6: The late fusion scheme for the two-stream Faster R-CNN framework.

Contributions beyond [9, 15, 16, 51] Xu et al. [51] did not exploit any context features in either proposal generation or action classification. Dai et al. [9] included context features when generating proposals, but used only the features within the proposal in action classification. Gao et al. exploited context features in either proposal generation only [16] or both stages [15]. However, they average-pooled the features within the context regions, while we use temporal convolutions and SoI pooling to encode the temporal structure of the features.

4.3. Late Feature Fusion

In action classification, most of the state-of-the-art methods [37, 30, 49, 7, 14] rely on a two-stream architecture, which parallelly processes two types of input—RGB frames and pre-computed optical flow—and later fuses their features to generate the final classification scores. We hypothesize such two-stream input and feature fusion may also play an important role in temporal action localization. Therefore we propose a *late fusion* scheme for the two-stream Faster R-CNN framework. Conceptually, this is equivalent to performing the conventional late fusion in both the proposal generation and action classification stage (Fig. 6). We first extract two 1D feature maps from RGB frames and stacked optical flow, respectively, using two different networks. We process each feature map by a distinct Segment

Proposal Network, which parallelly generates the logits for anchor classification and boundary regression. We use the element-wise average of the logits from the two networks as the final logits to generate proposals. For each proposal, we perform SoI pooling parallelly on both feature maps, and apply a distinct DNN classifier on each output. Finally, the logits for action classification and boundary regression from both DNN classifiers are element-wisely averaged to generate the final detection output.

Note that a more straightforward way to fuse two features is through an *early fusion* scheme: we concatenate the two 1D feature maps in the feature dimension, and apply the same pipeline as before (Sec. 4.1 and 4.2). We show by experiments that the aforementioned late fusion scheme outperforms the early fusion scheme.

Contributions beyond [9, 15, 16, 51] Xu et al. [51] only used a single-stream feature (C3D). Both Dai et al. and Gao et al. used two-stream features, but either did not perform fusion [16] or only tried the early fusion scheme [9, 15].

5. Experiments

Dataset We perform ablation studies and state-of-the-art comparisons on the temporal action detection benchmark of THUMOS'14 [22]. The dataset contains videos from 20 sports action classes. Since the training set contains only trimmed videos with no temporal annotations, we use the 200 untrimmed videos (3,007 action instances) in the validation set to train our model. The test set consists of 213 videos (3,358 action instances). Each video is on average more than 3 minutes long, and contains on average more than 15 action instances, making the task particularly challenging. Besides THUMOS'14, we separately report our results on ActivityNet v1.3 [5] at the end of the section.

Evaluation Metrics We consider two tasks: *action proposal* and *action localization*. For action proposal, we calculate Average Recall (AR) at different Average Number of Proposals per Video (AN) using the public code provided by [12]. AR is defined by the average of all recall values using tIoU thresholds from 0.5 to 1 with a step size of 0.05. For action localization, we report mean Average Precision (mAP) using different tIoU thresholds.

Features To extract the feature maps, we first train a two-stream "Inflated 3D ConvNet" (I3D) model [7] on the Kinetics action classification dataset [25]. The I3D model builds upon state-of-the-art image classification architectures (i.e. Inception-v1 [42]), but inflates their filters and pooling kernels into 3D, leading to very deep, naturally spatiotemporal classifiers. The model takes as input a stack of 64 RGB/optical flow frames, performs spatio-temporal convolutions, and extracts a 1024-dimensional feature as the output of an average pooling layer. We extract both RGB and optical flow frames at 10 frames per second (fps) as input to the I3D model. To compute optical flow, we use a FlowNet [11] model trained on artificially generated data followed by fine-tuning on the Kinetics dataset using an unsupervised loss [44]. After training on Kinetics we fix the model and extract the 1024-dimensional output of the average pooling layer by stacking every 16 RGB/optical flow frames in the frame sequence. The input to our action localization model is thus two 1024-dimensional feature maps—for RGB and optical flow—sampled at 0.625 fps from the input videos.

Implementation Details Our implementation is based on the TensorFlow Object Detection API [21]. In proposal generation, we apply anchors of the following scales: $\{1, 2, 3, 4, 5, 6, 8, 11, 16\}$, i.e. $K = 9$. We set the number of filters to 256 for all convolutional and fully-connected layers in the Segment Proposal Network and the DNN classifier. We add a convolutional layer with kernel size 1 to reduce the feature dimension to 256 before the Segment Proposal Network and after the SoI pooling layer. We apply Non-Maximum Suppression (NMS) with tIoU threshold 0.7 on the proposal output and keep the top 300 proposals for action classification. The same NMS is applied to the final detection output for each action class separately. The training of TAL-Net largely follows the Faster R-CNN implementation in [21]. We provide the details in the supplementary material.

Receptive Field Alignment We validate the design for receptive field alignment by comparing four baselines: (1) a single-tower network with no temporal convolutions (Single), where each anchor is classified solely based on the feature at its center location; (2) a single-tower network with non-dilated temporal convolutions (Single+TConv), which represents the default Faster R-CNN architecture; (3) a multi-tower network with non-dilated temporal convolutions (Multi+TConv); (4) a multi-tower network with dilated temporal convolutions (Multi+Dilated, the proposed architecture). All temporal ConvNets have two layers, both with kernel size 3. Here we consider only a single-steam feature (i.e. RGB or flow) and evaluate the generated proposal with AR-AN. The results are reported in Tab. 1 (top for RGB and bottom for flow). The trend is consistent on both features: Single performs the worst, since it relies only on the context at the center location; Single+TConv and Multi+TConv both perform better than Single, but still, suffer from irrelevant context due to misaligned receptive fields; Multi-Dilated outperforms the others, as the receptive fields are properly aligned with the span of anchors.

Context Feature Extraction We first validate our design for context feature extraction in proposal generation. Tab. 2 compares the generated proposals before and after incorporating context features (top for RGB and bottom for flow).

AN	10	20	50	100	200
Single	9.4	15.3	25.3	33.9	41.3
Single + TConv	12.9	20.0	30.3	37.6	44.0
Multi + TConv	13.4	20.6	31.1	38.1	43.7
Multi + Dilated	**14.0**	**21.7**	**31.9**	**38.8**	**44.7**
Single	11.0	18.0	28.9	36.8	43.6
Single + TConv	15.1	23.2	33.7	40.0	44.7
Multi + TConv	15.7	24.0	35.0	41.1	46.2
Multi + Dilated	**16.3**	**25.4**	**35.8**	**42.3**	**47.5**

Table 1: Results for receptive field alignment on proposal generation in AR (%). Top: RGB stream. Bottom: Flow stream.

AN	10	20	50	100	200
Multi + Dilated	14.0	21.7	31.9	38.8	44.7
Multi + Dilated + Context	**15.1**	**22.2**	**32.3**	**39.9**	**46.8**
Multi + Dilated	16.3	25.4	35.8	42.3	47.5
Multi + Dilated + Context	**17.4**	**26.5**	**36.5**	**43.3**	**48.6**

Table 2: Results for incorporating context features in proposal generation in AR (%). Top: RGB stream. Bottom: Flow stream.

tIoU	0.1	0.3	0.5	0.7	0.9
SoI Pooling	44.9	38.4	28.5	13.0	**0.6**
SoI Pooling + Context	**49.3**	**42.6**	**31.9**	**14.2**	**0.6**
SoI Pooling	49.8	45.7	37.4	**18.8**	0.7
SoI Pooling + Context	**54.3**	**48.8**	**38.2**	18.6	**0.9**

Table 3: Results for incorporating context features in action classification in mAP (%). Top: RGB stream. Bottom: Flow stream.

tIoU	0.1	0.3	0.5	0.7	0.9
RGB	49.3	42.6	31.9	14.2	0.6
Flow	54.3	48.8	38.2	18.6	**0.9**
Early Fusion	**60.5**	52.8	40.8	19.3	0.8
Late Fusion	59.8	**53.2**	**42.8**	**20.8**	**0.9**

Table 4: Results for late feature fusion in mAP (%).

We achieve higher AR on both streams after the context features are included. Next, given better proposals, we evaluate context feature extraction in action classification. Tab. 3 compares the action localization results before and after incorporating context features (top for RGB and bottom for flow). Similarly, we achieve higher mAP nearly at all AN values on both streams after including the context features.

Late Feature Fusion Tab. 4 reports the action localization results of the two single-stream networks and the early and late fusion schemes. First, the flow based feature outperforms the RGB based feature, which coheres with the common observations in action classification [37, 49, 7, 14]. Second, the fused features outperform the two single-stream features, suggesting the RGB and flow features complement each other. Finally, the late fusion scheme outperforms the early fusion scheme except at tIoU threshold 0.1, validating our proposed design.

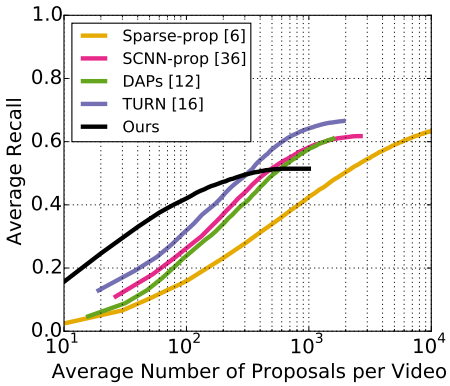

Figure 7: Our action proposal result in AR-AN (%) on THUMOS'14 comparing with other state-of-the-art methods.

tIoU	0.1	0.2	0.3	0.4	0.5	0.6	0.7
Karaman et al. [24]	4.6	3.4	2.4	1.4	0.9	–	–
Oneata et al. [32]	36.6	33.6	27.0	20.8	14.4	–	–
Wang et al. [47]	18.2	17.0	14.0	11.7	8.3	–	–
Caba Heilbron et al. [6]	–	–	–	–	13.5	–	–
Richard and Gall [34]	39.7	35.7	30.0	23.2	15.2	–	–
Shou et al. [36]	47.7	43.5	36.3	28.7	19.0	10.3	5.3
Yeung et al. [52]	48.9	44.0	36.0	26.4	17.1	–	–
Yuan et al. [54]	51.4	42.6	33.6	26.1	18.8	–	–
Escorcia et al. [12]	–	–	–	–	13.9	–	–
Buch et al. [3]	–	–	37.8	–	23.0	–	–
Shou et al. [35]	–	–	40.1	29.4	23.3	13.1	7.9
Yuan et al. [55]	51.0	45.2	36.5	27.8	17.8	–	–
Buch et al. [2]	–	–	45.7	–	29.2	–	9.6
Gao et al. [15]	60.1	56.7	50.1	41.3	31.0	19.1	9.9
Hou et al. [20]	51.3	–	43.7	–	22.0	–	–
Dai et al. [9]	–	–	–	33.3	25.6	15.9	9.0
Gao et al. [16]	54.0	50.9	44.1	34.9	25.6	–	–
Xu et al. [51]	54.5	51.5	44.8	35.6	28.9	–	–
Zhao et al. [56]	**66.0**	**59.4**	51.9	41.0	29.8	–	–
Ours	59.8	57.1	**53.2**	**48.5**	**42.8**	**33.8**	**20.8**

Table 5: Action localization mAP (%) on THUMOS'14.

State-of-the-Art Comparisons We compare TAL-Net with state-of-the-art methods on both action proposal and localization. Fig. 7 shows the AR-AN curves for action proposal. TAL-Net outperforms all other methods in the low AN region, suggesting our top proposals have higher quality. Although our AR saturates earlier as AN increases, this is because we extract features at a much lower frequency (i.e. 0.625 fps) due to the high computational demand of the I3D models. This reduces the density of anchors and lowers the upper bound of the recall. Tab. 5 compares the mAP for action localization. TAL-Net achieves the highest mAP when the tIoU threshold is greater than 0.2, suggesting it can localize the boundaries more accurately. We particularly highlight our result at tIoU threshold 0.5, where TAL-Net outperforms the state-of-the-art by 11.8% mAP (42.8%

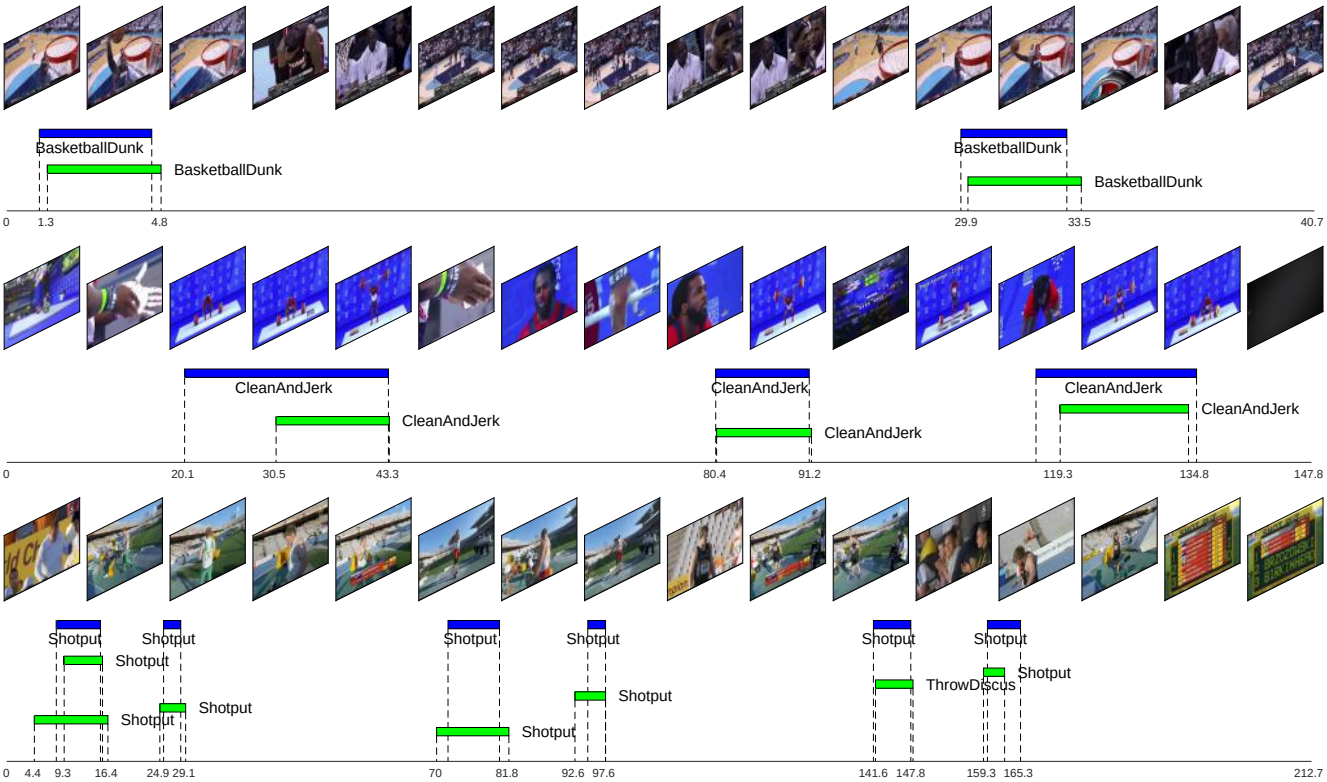

Figure 8: Qualitative examples of the top localized actions on THUMOS'14. Each consists of a sequence of frames sampled from a full test video, the ground-truth (blue) and predicted (green) action segments and class labels, and a temporal axis showing the time in seconds.

versus 31.0% from Gao et al. [15]).

Qualitative Results Fig. 8 shows qualitative examples of the top localized actions on THUMOS'14. Each consists of a sequence of frames sampled from a full test video, the ground-truth (blue) and predicted (green) action segments and class labels, and a temporal axis showing the time in seconds. In the top example, our method accurately localizes both instances in the video. In the middle example, the action classes are correctly classified, but the start of the leftmost prediction is inaccurate, due to subtle differences between preparation and the start of the action. In the bottom, "ThrowDiscus" is misclassified due to similar context.

Results on ActivityNet Tab. 6 shows our action localization results on the ActivityNet v1.3 validation set along with other recent published results. TAL-Net outperforms other Faster R-CNN based methods at tIoU threshold 0.5 (38.23% vs. 36.44% from Dai et al. [9] and 26.80% from Xu et al. [51]). Note that THUMOS'14 is a better dataset for evaluating action localization than ActivityNet, as the former has more action instances per video and each video contains a larger portion of background activity: on average, the THUMOS'14 training set has 15 instances per video and each video has 71% background, while the ActivityNet training set has only 1.5 instances per video and each video has only 36% background.

tIoU	0.5	0.75	0.95	Average
Singh and Cuzzolin [39]	34.47	–	–	–
Wang and Tao [50]	43.65	–	–	–
Shou et al. [35]	**45.30**	**26.00**	0.20	**23.80**
Dai et al. [9]	36.44	21.15	**3.90**	–
Xu et al. [51]	26.80	–	–	12.70
Ours	38.23	18.30	1.30	20.22

Table 6: Action localization mAP (%) on ActivityNet v1.3 (val).

6. Conclusion

We introduce TAL-Net, an improved approach to temporal action localization in video that is inspired by the Faster RCNN object detection framework. TAL-Net features three novel architectural changes that address three key shortcomings of existing approaches: (1) receptive field alignment; (2) context feature extraction; and (3) late feature fusion. We achieve state-ofthe-art performance for both action proposal and localization on THUMOS14 detection benchmark and competitive performance on ActivityNet challenge.

Acknowledgement We thank João Carreira and Susanna Ricco for their help on the I3D models and optical flow.

References

[1] https://github.com/yjxiong/action-detection. 11

[2] S. Buch, V. Escorcia, B. Ghanem, L. Fei-Fei, and J. C. Niebles. End-to-end, single-stream temporal action detection in untrimmed videos. In *BMVC*, 2017. 2, 7

[3] S. Buch, V. Escorcia, C. Shen, B. Ghanem, and J. C. Niebles. SST: Single-stream temporal action proposals. In *CVPR*, 2017. 2, 7

[4] F. Caba Heilbron, W. Barrios, V. Escorcia, and B. Ghanem. SCC: Semantic context cascade for efficient action detection. In *CVPR*, 2017. 2

[5] F. Caba Heilbron, V. Escorcia, B. Ghanem, and J. C. Niebles. ActivityNet: A large-scale video benchmark for human activity understanding. In *CVPR*, 2015. 2, 6

[6] F. Caba Heilbron, J. C. Niebles, and B. Ghanem. Fast temporal activity proposals for efficient detection of human actions in untrimmed videos. In *CVPR*, 2016. 2, 7

[7] J. Carreira and A. Zisserman. Quo vadis, action recognition? a new model and the Kinetics dataset. In *CVPR*, 2017. 2, 5, 6, 7

[8] L.-C. Chen, G. Papandreou, I. Kokkinos, K. Murphy, and A. L. Yuille. Semantic image segmentation with deep convolutional nets and fully connected CRFs. In *ICLR*, 2015. 4

[9] X. Dai, B. Singh, G. Zhang, L. S. Davis, and Y. Q. Chen. Temporal context network for activity localization in videos. In *ICCV*, 2017. 2, 3, 4, 5, 6, 7, 8

[10] A. Dave, O. Russakovsky, and D. Ramanan. Predictive-corrective networks for action detection. In *CVPR*, 2017. 2

[11] A. Dosovitskiy, P. Fischer, E. Ilg, P. Hausser, C. Hazirbas, V. Golkov, P. van der Smagt, D. Cremers, and T. Brox. FlowNet: Learning optical flow with convolutional networks. In *ICCV*, 2015. 6

[12] V. Escorcia, F. Caba Heilbron, J. C. Niebles, and B. Ghanem. DAPs: Deep action proposals for action understanding. In *ECCV*, 2016. 2, 6, 7

[13] M. Everingham, S. M. A. Eslami, L. Van Gool, C. K. I. Williams, J. Winn, and A. Zisserman. The PASCAL visual object classes challenge: A retrospective. *IJCV*, 111(1):98–136, Jan 2015. 1

[14] C. Feichtenhofer, A. Pinz, and R. P. Wildes. Spatiotemporal multiplier networks for video action recognition. In *CVPR*, 2017. 2, 5, 7

[15] J. Gao, Z. Yang, and R. Nevatia. Cascaded boundary regression for temporal action detection. In *BMVC*, 2017. 2, 3, 4, 5, 6, 7, 8

[16] J. Gao, Z. Yang, C. Sun, K. Chen, and R. Nevatia. TURN TAP: Temporal unit regression network for temporal action proposals. In *ICCV*, 2017. 2, 3, 4, 5, 6, 7

[17] R. Girshick. Fast R-CNN. In *ICCV*, 2015. 1, 2, 3, 5, 11

[18] R. Girshick, J. Donahue, T. Darrell, and J. Malik. Rich feature hierarchies for accurate object detection and semantic segmentation. In *CVPR*, 2014. 1, 2

[19] G. Gkioxari and J. Malik. Finding action tubes. In *CVPR*, 2015. 2

[20] R. Hou, R. Sukthankar, and M. Shah. Real-time temporal action localization in untrimmed videos by sub-action discovery. In *BMVC*, 2017. 2, 7

[21] J. Huang, V. Rathod, C. Sun, M. Zhu, A. Korattikara, A. Fathi, I. Fischer, Z. Wojna, Y. Song, S. Guadarrama, and K. Murphy. Speed/accuracy trade-offs for modern convolutional object detectors. In *CVPR*, 2017. 6

[22] Y.-G. Jiang, J. Liu, A. Roshan Zamir, G. Toderici, I. Laptev, M. Shah, and R. Sukthankar. THUMOS challenge: Action recognition with a large number of classes. http://crcv.ucf.edu/THUMOS14/, 2014. 2, 3, 6

[23] V. Kalogeiton, P. Weinzaepfel, V. Ferrari, and C. Schmid. Action tubelet detector for spatio-temporal action localization. In *ICCV*, 2017. 2

[24] S. Karaman, L. Seidenari, and A. D. Bimbo. Fast saliency based pooling of fisher encoded dense trajectories. http://crcv.ucf.edu/THUMOS14/, 2014. 1, 2, 7

[25] W. Kay, J. Carreira, K. Simonyan, B. Zhang, C. Hillier, S. Vijayanarasimhan, F. Viola, T. Green, T. Back, P. Natsev, M. Suleyman, and A. Zisserman. The Kinetics human action video dataset. *arXiv preprint arXiv:1705.06950*, 2017. 6

[26] C. Lea, M. Flynn, R. Vidal, A. Reiter, and G. Hager. Temporal convolutional networks for action segmentation and detection. In *CVPR*, 2017. 2, 4

[27] T. Lin, X. Zhao, and Z. Shou. Single shot temporal action detection. In *ACM Multimedia*, 2017. 2

[28] T.-Y. Lin, M. Maire, S. Belongie, J. Hays, P. Perona, D. Ramanan, P. Dollár, and C. Zitnick. Microsoft COCO: Common objects in context. In *ECCV*. 2014. 1

[29] S. Ma, L. Sigal, and S. Sclaroff. Learning activity progression in LSTMs for activity detection and early detection. In *CVPR*, 2016. 2

[30] J. Y.-H. Ng, M. Hausknecht, S. Vijayanarasimhan, O. Vinyals, R. Monga, and G. Toderici. Beyond short snippets: Deep networks for video classification. In *CVPR*, 2015. 1, 2, 5

[31] B. Ni, X. Yang, and S. Gao. Progressively parsing interactional objects for fine grained action detection. In *CVPR*, 2016. 2

[32] D. Oneata, J. Verbeek, , and C. Schmid. The LEAR submission at thumos 2014. http://crcv.ucf.edu/THUMOS14/, 2014. 1, 2, 7

[33] S. Ren, K. He, R. Girshick, and J. Sun. Faster R-CNN: Towards real-time object detection with region proposal networks. In *NIPS*. 2015. 1, 2, 3, 5, 11

[34] A. Richard and J. Gall. Temporal action detection using a statistical language model. In *CVPR*, 2016. 2, 7

[35] Z. Shou, J. Chan, A. Zareian, K. Miyazawa, and S.-F. Chang. Cdc: Convolutional-de-convolutional networks for precise temporal action localization in untrimmed videos. In *CVPR*, 2017. 2, 7, 8

[36] Z. Shou, D. Wang, and S.-F. Chang. Temporal action localization in untrimmed videos via multi-stage CNNs. In *CVPR*, 2016. 2, 7

[37] K. Simonyan and A. Zisserman. Two-stream convolutional networks for action recognition in videos. In *NIPS*. 2014. 1, 2, 5, 7

[38] B. Singh, T. K. Marks, M. Jones, O. Tuzel, and M. Shao. A multi-stream bi-directional recurrent neural network for fine-grained action detection. In *CVPR*, 2016. 2

[39] G. Singh and F. Cuzzolin. Untrimmed video classification for activity detection: submission to ActivityNet challenge. In *ActivityNet Large Scale Activity Recognition Challenge*, 2016. 8

[40] G. Singh, S. Saha, M. Sapienza, P. Torr, and F. Cuzzolin. Online real-time multiple spatiotemporal action localisation and prediction. In *ICCV*, 2017. 2

[41] C. Sun, S. Shetty, R. Sukthankar, and R. Nevatia. Temporal localization of fine-grained actions in videos by domain transfer from web images. In *ACM Multimedia*, 2015. 2

[42] C. Szegedy, W. Liu, Y. Jia, P. Sermanet, S. Reed, D. Anguelov, D. Erhan, V. Vanhoucke, and A. Rabinovich. Going deeper with convolutions. In *CVPR*, 2015. 6

[43] D. Tran, L. Bourdev, R. Fergus, L. Torresani, and M. Paluri. Learning spatiotemporal features with 3D convolutional networks. In *ICCV*, 2015. 2

[44] S. Vijayanarasimhan, S. Ricco, C. Schmid, R. Sukthankar, and K. Fragkiadaki. SfM-Net: Learning of structure and motion from video. *arXiv preprint arXiv:1704.07804*, 2017. 6

[45] C. Vondrick, D. Patterson, and D. Ramanan. Efficiently scaling up crowdsourced video annotation. *IJCV*, 101(1):184–204, Jan 2013.

[46] H. Wang and C. Schmid. Action recognition with improved trajectories. In *ICCV*, 2013. 1, 2

[47] L. Wang, Y. Qiao, and X. Tang. Action recognition and detection by combining motion and appearance features. `http://crcv.ucf.edu/THUMOS14/`, 2014. 1, 2, 7

[48] L. Wang, Y. Xiong, D. Lin, and L. Van Gool. Untrimmednets for weakly supervised action recognition and detection. In *CVPR*, 2017. 2

[49] L. Wang, Y. Xiong, Z. Wang, Y. Qiao, D. Lin, X. Tang, and L. Van Gool. Temporal segment networks: Towards good practices for deep action recognition. In *ECCV*, 2016. 2, 5, 7

[50] R. Wang and D. Tao. UTS at ActivityNet 2016. In *ActivityNet Large Scale Activity Recognition Challenge*, 2016. 8

[51] H. Xu, A. Das, and K. Saenko. R-C3D: Region convolutional 3D network for temporal activity detection. In *ICCV*, 2017. 2, 3, 4, 5, 6, 7, 8

[52] S. Yeung, O. Russakovsky, G. Mori, and L. Fei-Fei. End-to-end learning of action detection from frame glimpses in videos. In *CVPR*, 2016. 2, 7

[53] F. Yu and V. Koltun. Multi-scale context aggregation by dilated convolutions. In *ICLR*, 2016. 4

[54] J. Yuan, B. Ni, X. Yang, and A. A. Kassim. Temporal action localization with pyramid of score distribution features. In *CVPR*, 2016. 2, 7

[55] Z. Yuan, J. C. Stroud, T. Lu, and J. Deng. Temporal action localization by structured maximal sums. In *CVPR*, 2017. 2, 7

[56] Y. Zhao, Y. Xiong, L. Wang, Z. Wu, D. Lin, and X. Tang. Temporal action detection with structured segment networks. In *ICCV*, 2017. 2, 7, 11

A. Supplementary Material

A.1. Training Strategy

As in Faster R-CNN [33], the training of proposal generation and action classification share a same form of multi-task loss, targeting both classification and regression:

$$\mathcal{L} = \sum_i \mathcal{L}_{cls}(p_i, p_i^*) + \lambda \sum_i [p_i^* \geq 1] \mathcal{L}_{reg}(t_i, t_i^*). \quad (1)$$

i is the index of an anchor or proposal in a mini-batch. For classification, p is the predicted probability of the proposal or actions, p^* is the ground-truth label, and $\mathcal{L}_{cls}$ is the cross-entropy loss. Note that $p^* \in \{0, 1\}$ for proposal generation, and $p^* \in \{0, \ldots, C\}$ for action classification, where C is the number of action classes of interest and 0 accounts for the background action class. For regression, t is the predicted offset relative to an anchor or proposal, t^* is the ground-truth offset, and $\mathcal{L}_{reg}$ is the smooth L1 loss defined in [17]. We parameterize the offsets $t = (t_c, t_l)$ and $t^* = (t_c^*, t_l^*)$ by:

$$\begin{aligned} t_c &= 10 \cdot (c - c_a)/c_i, \quad & t_l &= 5 \cdot \log(l/l_a), \\ t_c^* &= 10 \cdot (c^* - c_a)/c_i, \quad & t_l^* &= 5 \cdot \log(l^*/l_a), \end{aligned} \quad (2)$$

where c and l denote the segment's center coordinate and its length. c and c^* account for the predicted and ground-truth segments, while c_a accounts for the anchor and proposal segments, for proposal generation and action classification, respectively (similarly for l). The indicator function $[\cdot]$ is used to exclude the background anchors and proposals when the regression loss is computed. In all experiments, we set $\lambda = 1$ for both proposal generation and action classification, and jointly train both stages by weighing both losses equally.

For proposal generation, an anchor is assigned a positive label if it overlaps with a ground-truth segment with temporal Intersection-over-Union (tIoU) higher than 0.7. A negative label is assigned if the tIoU overlap is lower than 0.3 with all ground-truth segments. We also force each ground-truth segment to have at least one matched positive anchor. For action classification, a proposal is assigned the action label of its most overlapped ground-truth segment, if the ground-truth segment has tIoU overlap over 0.5. Otherwise a background label (i.e. 0) is assigned.

Each mini-batch contains examples sampled from a single video. For proposal generation, we set the mini-batch size to 256 and the fraction of positives to 0.5. For action classification, we set the mini-batch size to 64 and the fraction of foreground actions to 0.25. We use the Adam optimizer with a learning rate of 0.0001.

A.2. Additional Qualitative Results

Besides Fig. 8, we show additional qualitative examples on THUMOS'14 in Fig. 9 and 10. Our approach successfully localizes the actions in most cases. The failure cases include: (1) inaccurate boundaries, e.g. Fig. 8 (middle), (2) misclassified actions, e.g. Fig. 8 (bottom) and Fig. 9 (a), (3) false positives due to indistinguishable body motions, e.g. Fig. 9 (b) and Fig. 10 (c), and (4) false negatives due to small objects and occlusion, e.g. Fig. 9 (d).

	InceptionV3 RGB (ImageNet pre-trained)
Zhao et al. [56]	18.3
Ours	**26.0**

Table 7: Action localization mAP (%) on THUMOS'14 using InceptionV3. The result of [56] is copied from [1].

Step	Running Time (ms)	
Optical Flow	239	per frame
I3D Features	825	per 16 frame input
Proposal + Classification	9	per 3000 frames

Table 8: Running time (ms) of each step during test time.

A.3. Benchmarks using InceptionV3

Besides I3D features, we also evaluate our method with features extracted from an InceptionV3 model pre-trained on ImageNet. This provides an apples-to-apples comparison with the result of Zhao et al. [56] reported in [1]. Tab. 7 shows the action localization mAP on THUMOS'14. Our approach outperforms Zhao et al. [56] by 7.7% in mAP, validating the effectiveness of our proposed architecture.

A.4. Computational Cost

Tab. 8 shows a running time breakdown during the test time for the following three steps: (1) optical flow extraction, (2) I3D feature extraction, and (3) proposal and classification. All these running time experiments are performed on CPUs, so further speedup is possible with GPU devices. The computational bottleneck is on the optical flow extraction (i.e. 239 ms per frame).

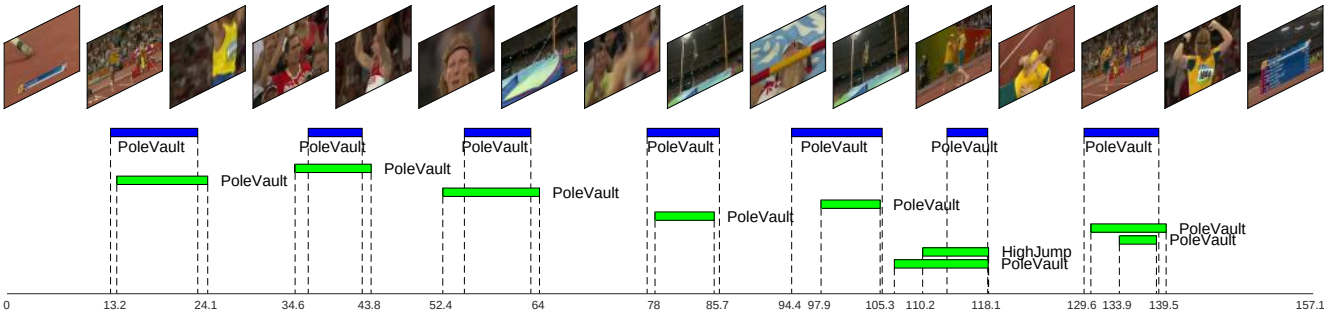

(a)

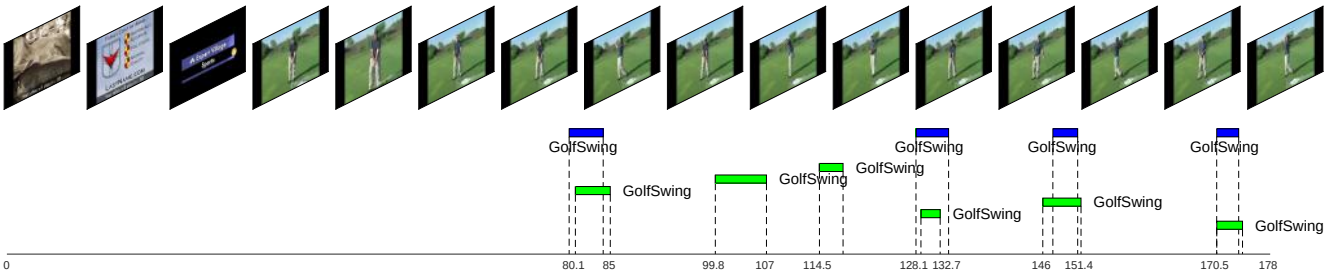

(b)

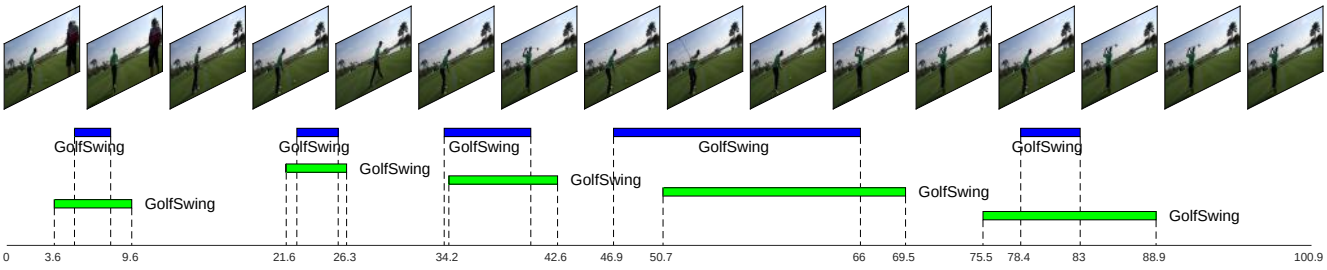

(c)

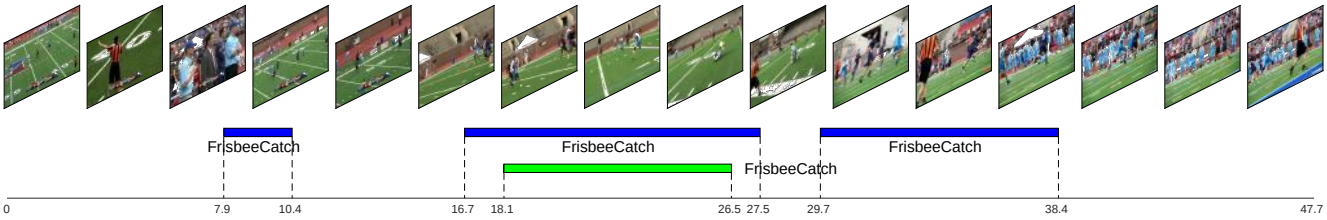

(d)

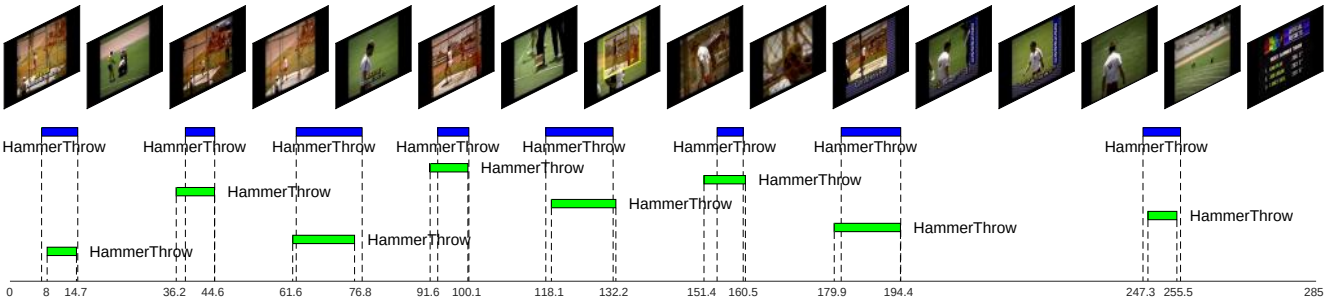

(e)

Figure 9: Additional qualitative examples of the top localized actions on THUMOS'14. Each consists of a sequence of frames sampled from a full test video, the ground-truth (blue) and predicted (green) action segments and class labels, and a temporal axis showing the time in seconds.

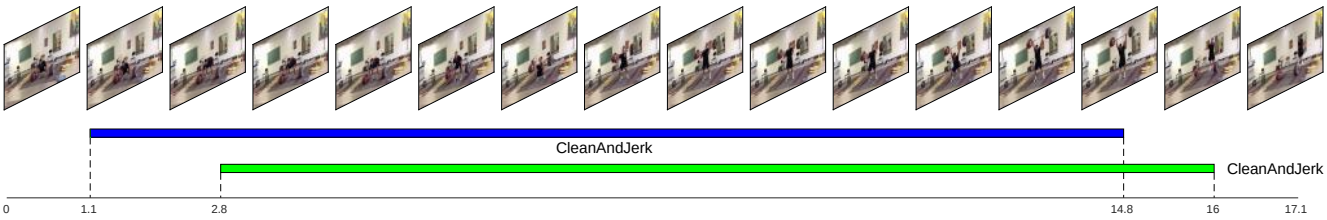

(a)

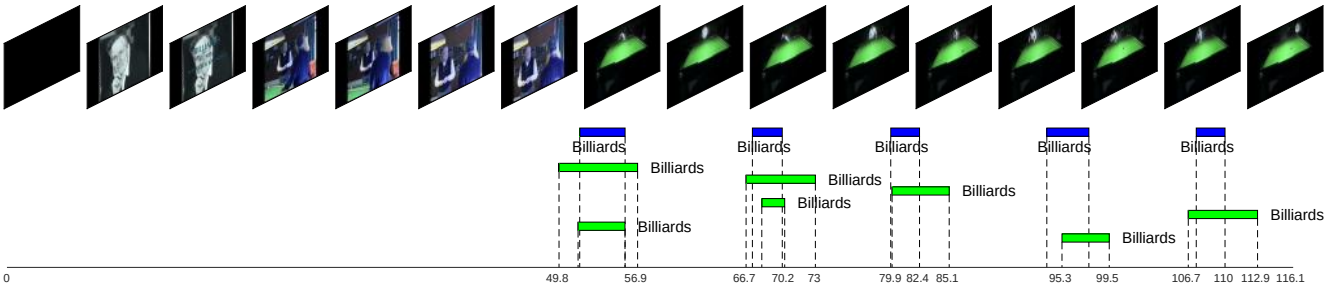

(b)

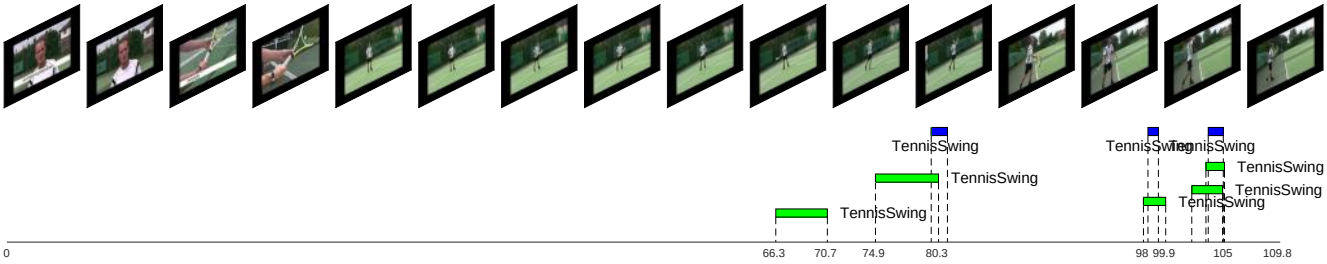

(c)

(d)

Figure 10: Additional qualitative examples of the top localized actions on THUMOS'14. Each consists of a sequence of frames sampled from a full test video, the ground-truth (blue) and predicted (green) action segments and class labels, and a temporal axis showing the time in seconds.